

Tetrahedral Hohltraums—An Alternative Approach to Indirect Drive on OMEGA and the NIF

The preceding article reported on the first indirect-drive experiments carried out on OMEGA, using cylindrical hohlraums. This article advocates the use of tetrahedral hohlraums, by which are understood spherical hohlraums with four laser entrance holes (LEH's) placed at or near the vertices of a tetrahedron. This alternative approach appears to be well suited to the OMEGA geometry and could offer an alternate route to ignition on the National Ignition Facility (NIF).

The primary advantage provided by the tetrahedral hohlraum is better radiation uniformity on the capsule. Historically, the cylindrical hohlraum¹ has been the preferred approach. Among the reasons for this may be that the cylindrical geometry is two-dimensional (2-D) and therefore permits detailed hydrodynamic modeling and optimization, while the tetrahedral hohlraum is intrinsically 3-D and thus not amenable to modeling with currently available hydrodynamic codes. However, a comparison between the two approaches is now possible using a new, 3-D view-factor code named *BUTTERCUP*. While this code does not include any hydrodynamics, it does enable reasonable predictions to be made for cylindrical and tetrahedral hohlraums on both OMEGA and the NIF.

On OMEGA, the target chamber geometry provides an exact tetrahedral symmetry, permitting the irradiation of tetrahedral hohlraums with all 60 beams. In comparison, only 40 beams can be used for cylindrical hohlraums. For the NIF, assuming that 72 ports are provided to accommodate direct drive (as is the current baseline), it will be possible to irradiate a tetrahedral hohlraum with 44 out of the 48 beams without in any way compromising the geometrical arrangement of beams required for cylindrical hohlraums or direct drive. On both laser systems, *BUTTERCUP* predicts that good irradiation uniformity ($\sim 2\%$ rms) will be obtained on the capsule at all times during the implosion. This uniformity is relatively insensitive to albedo and other changing conditions inside the hohlraum. "Beam phasing" (the use of different temporal pulse shapes in different beams), which is required for cylindrical hohlraums, may not be necessary for tetrahedral hohlraums.

The cylindrical and tetrahedral geometries considered in this article are shown in Fig. 68.9. Each type of hohlraum can be irradiated on each laser system. The z axis is taken to lie along the hohlraum axis for conventional cylindrical hohlraums. This corresponds to the true vertical direction for the NIF, and to a pent-pent axis for the experiments on OMEGA described in the preceding article. The cylindrical hohlraum for OMEGA is a scale-1 Nova hohlraum. The tetrahedral hohlraums are viewed from different angles—from the vertical for the NIF and along a hex-hex axis for OMEGA. For tetrahedral hohlraums on OMEGA, each LEH faces a hexagon on the target chamber located at a vertex of a regular tetrahedron. The target chamber geometry permits ten distinct orientations of the hohlraum.

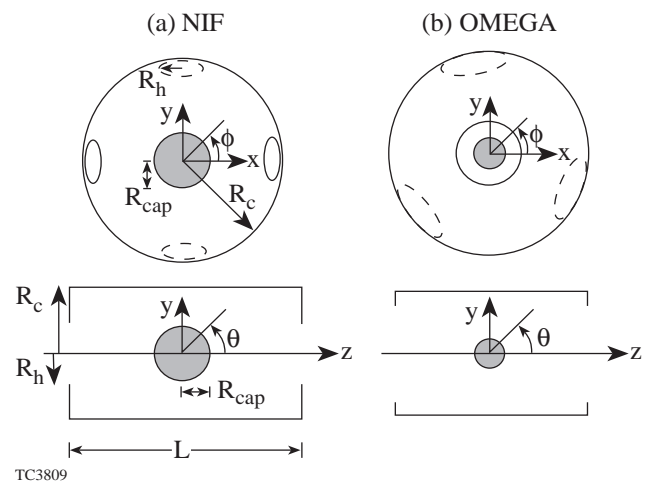


Figure 68.9
Tetrahedral and cylindrical hohlraums for (a) the NIF and (b) OMEGA with the capsule shown shaded. For each laser system the two hohlraums are drawn to the same scale. Tetrahedral hohlraums for the NIF are viewed from the vertical (z) direction and have laser entrance holes (LEH's) at $\theta = 55^\circ$ and 125° . Those for OMEGA are viewed from one LEH, taken to define the z axis, and the other LEH's are arranged in tetrahedral symmetry with $\theta = 109.5^\circ$; each LEH is aligned with a hexagonal face of the target chamber.

This article will review the issue of indirect-drive uniformity, describe the code *BUTTERCUP*, and present results for OMEGA and the NIF. Given the demonstrated ability of the OMEGA laser to perform precision indirect-drive experiments, as described in the preceding article, it is clear that OMEGA is uniquely capable of investigating the feasibility of tetrahedral hohlraums.

Indirect-Drive Uniformity

Many issues are crucial for the success of indirect-drive ICF. These include ensuring a high conversion efficiency of laser energy to x rays, ensuring that the laser energy can enter the hohlraum unimpeded by plasma ablating from around the laser entrance holes (LEH's), avoiding absorption of the laser energy into low-density plasma whether from the capsule or the wall, avoiding laser-plasma instabilities, tailoring the radiation drive on the capsule by designing a suitably shaped laser pulse, and maximizing the energy coupling into the capsule by making the capsule as large as possible and the LEH's as small as possible relative to the dimensions of the case. However, the most critical issue may be that of ensuring an acceptable level of radiation drive uniformity on the capsule.

In the standard cylindrical hohlraum, the uniformity issue is indeed critical. On the Nova laser at the Lawrence Livermore National Laboratory, for example, there are ten laser beams, five through each LEH, whose irradiation pattern on the inside of the case may be represented as two rings in a cylindrically symmetric geometry. In reality, of course, there are ten more or less distinct laser spots with some azimuthal asymmetry. The uniformity experienced by the capsule varies in three stages: (a) initially, the x-ray flux arises predominantly from the laser-irradiated spots; (b) later, the hohlraum wall "warms up," contributing a component with deficits at the poles of the capsule (the points that face the LEH's); and (c) still later, as plasma expands from the curved portion of the case, the laser energy is absorbed closer to the LEH's, an effect known as spot motion, and the component due to the laser-heated spots develops a surplus at the poles. These three stages of time-dependent uniformity have been well documented.¹⁻³ While these time-dependent nonuniformities may average out to a certain extent,¹ it is desirable to maintain good uniformity throughout the implosion. According to Refs. 1 and 4, the tolerable level of time-dependent nonuniformity may be of the order of 4%–10%, depending on the details of the target design, as long as the time-averaged uniformity is $\leq 1\%$. (In Ref. 5, however, it is asserted, based on a simplified, thin-shell hydrodynamic model, that time-dependent asymmetries should not exceed $\pm 2\%$.) Another effect—laser-beam steering in gas-filled hohlraums

(hohlraums filled with low-density, low- Z gas intended to prevent high- Z plasma from the walls from filling the hohlraum^{1,4})—has also been identified as significant.⁶

In the base-line design⁴ for a cylindrical hohlraum on the NIF, the 48 beams (each a two-by-two array of sub-beams) are arranged on the target chamber in eight rings, each corresponding to a different angle θ with respect to the vertical (z) direction in the target area. When focused onto the hohlraum wall, the rings overlap in pairs, so that the inner surface of the hohlraum is effectively irradiated with two rings in each of the north and south hemispheres. By varying the relative powers of the different rings ("beam phasing"),¹ it is possible to eliminate the P_2 spherical-harmonic component of irradiation nonuniformity on the capsule at all times and the P_4 component in the time-averaged sense. The desired beam power histories may be obtained through "integrated calculations," which include the two-dimensional hydrodynamic evolution of the hohlraum (assumed azimuthally symmetric) and detailed radiation transport.

The P_2 component of nonuniformity is avoided entirely in tetrahedral hohlraums. Using a geometric treatment, Phillion and Pollaine⁷ found that with strict tetrahedral symmetry, all $l = 1, 2,$ and 5 spherical-harmonic components are identically zero, regardless of spot motion, beam steering, or other real physical effects; in addition, with a combination of judiciously selected beam locations and beam phasing, the $l = 3$ and 4 components can be made to vanish at all times. Tetrahedral hohlraums thus offer improved uniformity compared with cylindrical hohlraums. Possible drawbacks include the following: (a) beam placements designed with true tetrahedral symmetry as in Ref. 7 would be incompatible with cylindrical hohlraums and thus with the NIF; (b) the hydrodynamics are harder to model as the configuration is 3-D rather than 2-D; (c) with four holes rather than two, there may be more radiation losses; and (d) there may be more LEH clearance problems. The trade-off between these issues remains to be resolved. However, on the basis of uniformity considerations, this article suggests that the tetrahedral hohlraum may be a viable approach worth pursuing on the NIF, complementary to the cylindrical hohlraum.

Aside from Ref. 7, the tetrahedral geometry has been studied previously only to a limited extent. To the best of our knowledge, Azechi⁸ was the first to describe it in the ICF literature. In this reference, the target was conceived as a "cannonball" target, in which the capsule would be imploded not by x rays but by the plasma ablated off the inside of the hohlraum wall. Spherical cannonball targets with 2, 4, and 12 holes are

described in Ref. 9, which also presents some tomographic x-ray images of the compressed core.

The cannonball approach was dropped in favor of the radiation-drive approach, where, for reasons of uniform capsule drive, it is necessary to avoid the wall plasma contributing to the drive on the capsule. For many years radiation drive was conceived in the literature as occurring with a spherical radiation case. (In 1990, though, Kato¹⁰ published experimental work on cylindrical hohlraums that clearly demonstrated the importance of the $\ell = 2$ nonuniformity.) Mochizuki¹¹ considered two concentric spherical surfaces and calculated the geometrical smoothing associated with radiation emission from the outer to the inner surface. Murakami¹² extended this approach to use a spherical-harmonic decomposition of the radiation source on the case—each spherical-harmonic mode is damped by some appropriate factor to give the smoothed radiation drive on the capsule. Murakami gave examples for two-hole spherical hohlraums but did not include the contributions from portions of the case not irradiated directly by the laser beams; thus he did not consider nonuniformities on the capsule resulting from the finite size of the LEH's. The spherical-harmonic approach was also used in Ref. 7. Wilson¹³ considered three- and four-hole spherical hohlraums from the point of view of distributing the laser-irradiated spots as uniformly as possible on the interior of the hohlraum wall. Murakami¹⁴ used a view-factor code, close in spirit to the present work, to calculate the on-capsule uniformity in ellipsoidal and spherical cavities for ion-beam and laser drivers, respectively. Other work on radiation symmetrization is found in Ref. 15, which includes a model of the radiative heat wave moving into the wall; Ref. 16, which also considers a cylindrical hohlraum; and Ref. 17, which includes a treatment of the unirradiated hohlraum wall using a multiple-reemission smoothing factor.

The Code BUTTERCUP

The primary tool used in this article is the 3-D view-factor code *BUTTERCUP*. This code has been used to generate designs for cylindrical and tetrahedral hohlraums on both the NIF and the OMEGA laser systems. It considers the geometries shown in Fig. 68.9, which also serves to define some notation (the case radius R_c , the hole radius R_h , the capsule radius R_{cap} , and the conventional spherical angles θ and ϕ).

The code starts by tracing rays in 3-D from each laser beam, through the LEH's, and into the hohlraum. The rays are represented using a 2-D grid that covers the beam cross section. Typical beam paths into tetrahedral and cylindrical hohlraums

are shown in Fig. 68.10. Each beam is calculated independently, allowing for independent energies, pointings, etc. No symmetries are assumed. The NIF beams are assumed to derive from phase plates and to comprise parallel rays in the far field with a $500 \times 1000\text{-}\mu\text{m}$ elliptical cross section,⁴ oriented so that their intersections with the planes of the LEH's are approximately circular. The size of the cross section is determined from plasma physics considerations: i.e., smaller spots, while preferable for fitting through the LEH's, result in laser intensities (especially near the LEH's) that may be too high from the point of view of plasma instabilities. For OMEGA, phase plates are not assumed, but the beams are assumed to be focused through vacuum just outside the hohlraums, as is currently done on Nova. (The standard direct-drive phase plates on OMEGA have best-focus spot sizes of $\sim 0.8\text{ mm}$ —too large for indirect drive.)

The code is written to follow each ray through multiple reflections within the hohlraum, depositing some fraction $A(\theta_i)$

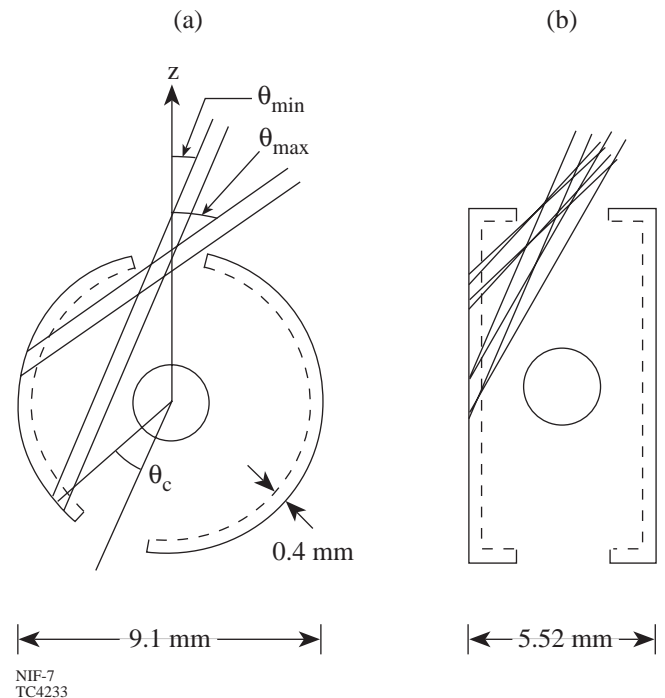


Figure 68.10
Representative beam paths into (a) tetrahedral and (b) cylindrical hohlraums, with dimensions appropriate to the NIF. In tetrahedral hohlraums the laser spots are spread fairly uniformly on the hohlraum wall, while in cylindrical hohlraums they lie on a small number of discrete rings. To account in a simple way for wall motion, the solid and dashed lines indicate the initial and final wall locations. For the tetrahedral hohlraums, the beams incident with θ_{min} and θ_{max} are drawn to illustrate clearance issues. One of these beams is drawn with a clearance angle θ_c from an opposing LEH. For an LEH angle $\theta_{LEH} = 55^\circ$, $\theta_{min} = 23.0^\circ$, $\theta_{max} = 54.8^\circ$, and the smallest $\theta_c = 23.7^\circ$.

each time where θ_i is the angle of incidence. The code can also impose a random scattering on the reflected rays, e.g., with a deflection cone having a specified shape and angular width. The code can be used to investigate glint—the early-time reflection of laser light from the hohlraum wall to the capsule. However, for the work presented here, the simple assumption is made that $A(\theta) = 1$. This should be a very good approximation for the large hohlraums of current interest, and especially for NIF hohlraums. For hohlraums on Nova, the absorption has been measured to be in excess of 90%.¹⁸ The main physical process not modeled here is distributed absorption along the ray path. This is especially important for hohlraums that are initially empty (i.e., not gas filled), in which the light can be absorbed at low densities in the ablating gold plasma whose expansion is unimpeded.

After all of the rays have been traced, *BUTTERCUP* calculates a background radiation temperature T_r that is spatially independent. The radiation field within the hohlraum is then treated as a Planckian distribution at this temperature. Experimentally, this is a rather good approximation.¹⁹ The temperature T_r at a given time is calculated using a simple, global energy balance between the power entering the radiation field from the laser source and the power lost from the radiation field, there being insignificant energy stored in the radiation field:

$$P_{\text{las}}(1 - \beta_l) = \sigma T_r^4 (\beta_c A_c + N A_h + \beta_w A_w), \quad (1)$$

where P_{las} is the total laser power absorbed by the case, β_l is the fraction of this power that is not converted to x rays, σ is Planck's constant, and the term $(\beta_c A_c + N A_h + \beta_w A_w)$ may be thought of as the effective area of the hohlraum. The quantities A_c , A_h , and A_w are the areas of the capsule, an LEH, and the wall, respectively, in a hohlraum with N holes. The quantity β_w is defined as $1 - \alpha_w$, where α_w is the wall albedo defined as the fraction of the x-ray energy incident on the hohlraum wall that is reradiated into the hohlraum; $\beta_c (= 1 - \alpha_c)$, where α_c is the capsule albedo) is similarly defined. The wall albedo α_w increases with time and, at the peak of the laser pulse, is typically 0.8 for Nova or OMEGA and 0.9 for the NIF. The capsule albedo α_c is taken here to be small (0.1); reemission from the capsule is in any case a minor factor in Eq. (1). The x-ray conversion efficiency, $1 - \beta_l$, depends on the irradiation conditions¹ and is taken to be 0.7 here.

Given the background temperature T_r , the emission intensity I_e (power per unit area) at any point on the interior of the case can be calculated from local energy balance. Incoming

fluxes comprise radiation from the cavity (σT_r^4) and the absorbed laser energy I_l . Subtracting the respective fractions β_w and β_l that are not re-radiated, one finds I_e :

$$I_e = (1 - \beta_w) \sigma T_r^4 + (1 - \beta_l) I_l. \quad (2)$$

One can then define an effective radiation temperature T_e by equating I_e to σT_e^4 , and, more important from the point of view of the code, the brightness (power per unit area per unit solid angle) $B = I_e / \pi$ at all points on the hohlraum wall.

At present, the code assumes that the albedos are spatially independent. This is not an intrinsic limitation since *BUTTERCUP* could easily be linked to some model giving the spatially dependent albedos through Eqs. (1) and (2). Another assumption implicit in the code is that the x-ray conversion efficiency is independent of the angle of incidence of the laser beams. Greater accuracy here would require a self-consistent hydrodynamic calculation.

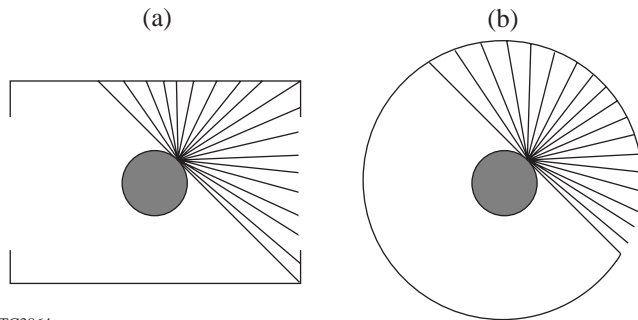
Given the brightness distribution B on the wall, *BUTTERCUP* then scans over a number of points on the capsule and, for each point (θ, ϕ) , determines the incoming irradiation intensity $I(\theta, \phi)$ by integrating the brightness over all angles (see Fig. 68.11). *BUTTERCUP* makes use of the fundamental result that, for radiation transport in vacuum, the spectral brightness is constant along a ray;²⁰ it thus suffices to follow each ray from the capsule, with spherical coordinates (θ', ϕ') relative to the capsule normal, to its intersection point on the wall and look up the brightness there. The incoming intensity is then given by

$$I(\theta, \phi) = \iint B(\theta', \phi') \cos \theta' \sin \theta' d\theta' d\phi'. \quad (3)$$

The $\cos \theta'$ factor accounts for the angle between a surface element of the capsule and the incoming ray, and the $\sin \theta'$ factor for the solid angle. The code does not split each of the outer and inner surfaces into segments for which cross-coupling coefficients are calculated, as is generally done in view-factor codes.¹⁴ Thus, while *BUTTERCUP* is known loosely as a view-factor code, “direct integration” would be a better description of its algorithm. The difference between the two approaches is minor; both approaches should give the same answers within the limits of numerical resolution.

Examples of *BUTTERCUP* predictions are given in Fig. 68.12 for tetrahedral hohlraums on OMEGA and the NIF. One-dimensional lineouts of the intensity on the capsule are shown as functions of azimuthal angle ϕ for various values of

θ , as are lineouts along θ for various values of ϕ . The symmetries shown in Fig. 68.9 are easily seen in the azimuthal scans. In Fig. 68.12(a) the scans at $\theta=45^\circ$ and 135° reflect the two-



TC3864

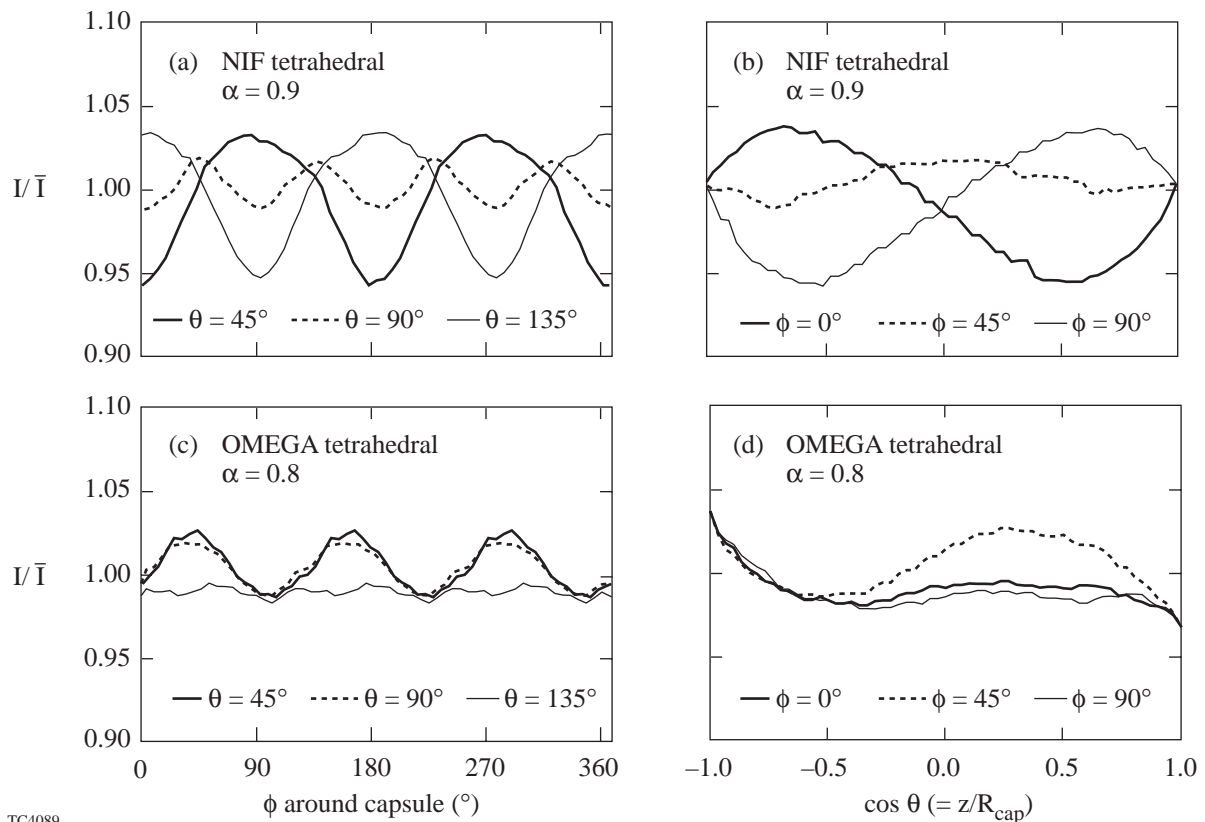
Figure 68.11
Schematic of the algorithm used by the view-factor code *BUTTERCUP*. The radiation flux incident at each point on the capsule is determined by integrating the brightness $B = \sigma T_e^4 / \pi$ of the wall over a hemispherical solid angle. The algorithm is essentially independent of whether the hohlraum is (a) cylindrical or (b) tetrahedral.

fold symmetry of the NIF, while the scan around the equator ($\theta=90^\circ$) shows a four-fold symmetry. For the OMEGA geometry, the expected three-fold symmetry is seen. In all cases the intensity minima correspond to points on the capsule facing an LEH.

Tetrahedral Hohlräume on OMEGA

A comparison has been made between cylindrical and tetrahedral hohlraums on OMEGA, using the parameters listed in Table 68.II. The cylindrical hohlraums are standard Nova hohlraums, except that slightly smaller LEH's are used.

As in the preceding article, the cylindrical hohlraums are conveniently irradiated with the axis of the cylinder oriented to pass through the centers of opposing pentagons on the target chamber. This provides, for each LEH, two rings of five beams with angles of incidence 21.4° and 42.0° , and a ring of ten beams at 58.9° . Figure 68.13 shows a possible design with beams pointed onto three rings on the cylinder wall. This combination of beams can deliver 20 kJ of energy in a 1.0-ns pulse.



TC4089

Figure 68.12
Representative results from *BUTTERCUP* calculations. The radiation intensity on the capsule is plotted against ϕ and $\cos\theta$ for NIF and OMEGA tetrahedral hohlraums. The different patterns correspond to the different orientations shown in Fig. 68.9. In all cases the minima occur at points facing the LEH's.

Table 68.II: Dimensions of cylindrical and tetrahedral hohlraums for the NIF and for OMEGA as used in this article. (In calculations where wall motion is included, these are the initial dimensions.)

| | | NIF | | OMEGA | |
|-----------------|--------------------------|-------------|-------------|-------------|-------------|
| | | Cylindrical | Tetrahedral | Cylindrical | Tetrahedral |
| Case radius | R_c (mm) | 2.76 | 4.55 | 0.8 | 1.4 |
| Hole radius | R_h (mm) | 1.38 | 1.14 | 0.5 | 0.4 |
| Length | L (mm) | 10.4 | — | 3.0 | — |
| Capsule radius | R_{cap} (mm) | 1.13 | 1.13 | 0.2 | 0.2 |
| | R_{cap}/R_c | 0.41 | 0.25 | 0.25 | 0.14 |
| Case area | A_c (mm ²) | 216.2 | 243.8 | 17.53 | 22.62 |
| Total hole area | A_h (mm ²) | 11.96 | 16.33 | 1.57 | 2.01 |
| | A_h/A_c | 0.055 | 0.067 | 0.09 | 0.09 |
| Energy | (kJ) | 1800 | 1650 | 20 | 30 |

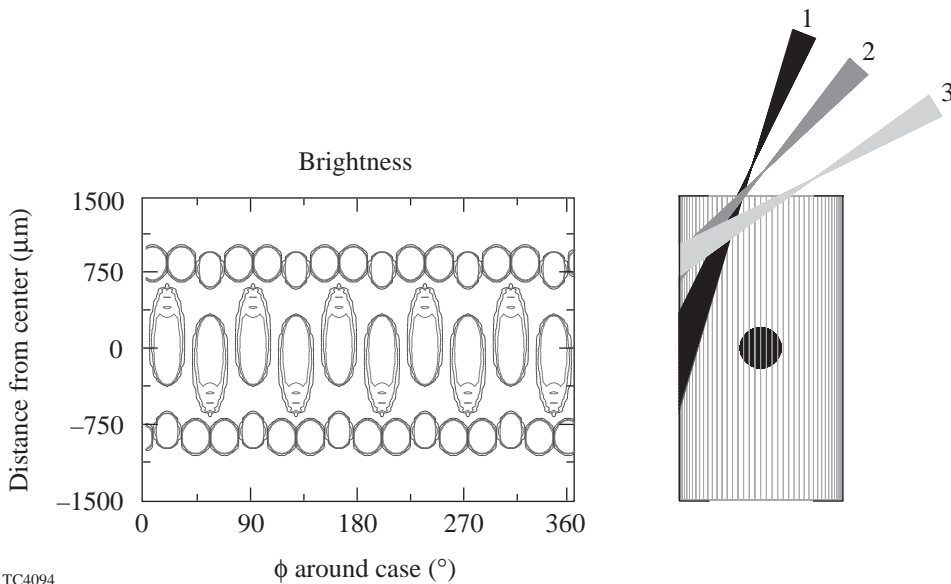


Figure 68.13

A possible irradiation geometry for cylindrical hohlraums on OMEGA (right) and corresponding contours of brightness B (left). A 40-beam subset of the 60 beams is used, comprising three different rings from each hemisphere of the target chamber. The inner and middle rings (1 and 2) possess five beams each, while the outer rings (3) have ten beams spaced in five pairs around the azimuth. The resulting pattern on the hohlraum wall comprises three bands, two with 15 beams each (as used in most of the experiments described in the preceding article) and one with ten beams.

TC4094

With a tetrahedral hohlraum, however, all 60 beams can be used for a total of 30 kJ of laser energy. The four groups of 15 beams entering the four LEH's are equivalent to each other with respect to rotations within the tetrahedral group. Through each LEH there are two sets of six beams, with $\theta = 23.2^\circ$ and 47.8° , respectively, and one set of three beams with $\theta = 58.8^\circ$.

A sinusoidal map (Fig. 68.14) of the locations of all 60 OMEGA beams on the wall of a tetrahedral hohlraum shows generally uniform coverage of the wall. The beams clear the LEH's with minimum clearances of $50 \mu\text{m}$ upon entering the case and $150 \mu\text{m}$ on the inside of the case.

The dependence of the rms nonuniformity σ_{rms} on albedo is shown in Fig. 68.15 for both cylindrical and tetrahedral hohlraums on OMEGA. Low albedo corresponds to early times, while the maximum albedo corresponds to the peak of the pulse or later times. For each type of hohlraum, one curve applies to "full power," i.e., equal beam energies, and the other to a "tuned" case, i.e., with the energy in some beams being reduced. The tuning carried out here is time independent; thus, the beams have different energies but the same pulse shape. (By appropriate detuning of the frequency-conversion crystals, this can probably be accomplished quite accurately on OMEGA.) For both cylindrical and tetrahedral hohlraums the

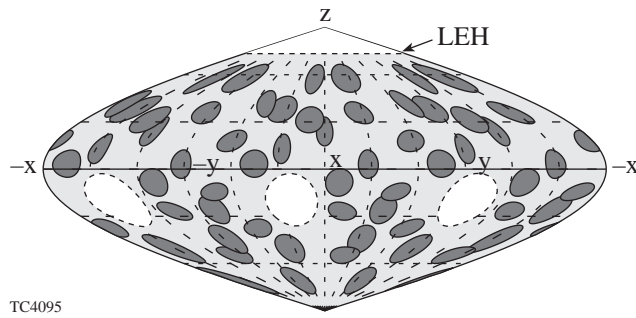


Figure 68.14

Sinusoidal map of the locations of all 60 OMEGA beam spots on the interior wall of a tetrahedral hohlraum. One LEH is centered on the z axis [as in Fig. 68.9(b)] and the others are shown as dashed circles. The exact tetrahedral symmetry of the OMEGA beam locations and the even distribution of beam spots on the hohlraum wall effectively eliminate all spherical harmonic modes other than those present in true tetrahedral geometry.

tuning was carried out to optimize the uniformity at or near the end of the laser pulse, where the albedo is approximately 0.8. Tuning the tetrahedral hohlraum was accomplished by noting that the symmetry of the system results in five groups of beams and adjusting the five available independent parameters.

Figure 68.15 shows a strong dependence of σ_{rms} on albedo (and thus time) in the case of the cylindrical hohlraum. While the tuned case performs significantly better, the time-dependent nonuniformity (dominated by the P_2 mode) is still evident. In contrast, the insensitivity to albedo for the tetrahedral hohlraum is striking. The reason is clear from Fig. 68.14—the laser spots are distributed so uniformly around the case that the contribution to the capsule uniformity due to the direct laser source shares the same intrinsic spatial distribution as the background radiation source. Thus, as the increasing albedo changes the proportions of these two sources, the net effect seen by the capsule is essentially zero. Using the same argument, it is probable that this picture will be unaffected by other effects such as wall motion, beam steering, and laser-beam refraction. It is hard to conceive of any processes that can systematically upset the uniform distribution of laser spots on the hohlraum wall.

The tuned tetrahedral curve exhibits some further improvement. This is achieved by increasing the relative weighting of beams near the LEH's, which results in a greater effect at early times. The tuned tetrahedral hohlraum achieves a total rms nonuniformity of 1.5% or less throughout the whole range of albedos. The slightly better performance of the OMEGA

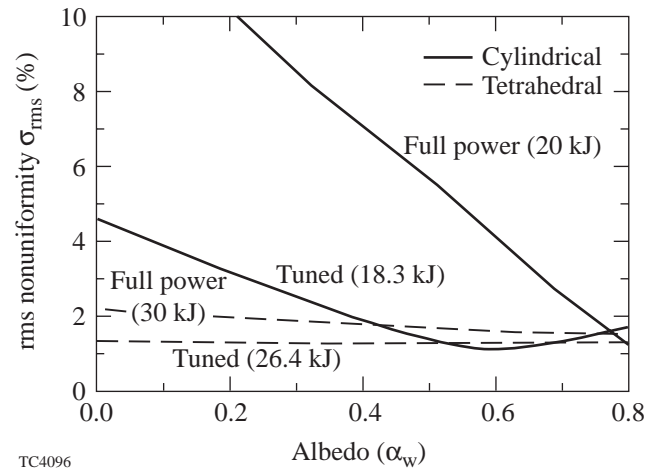


Figure 68.15

Nonuniformity σ_{rms} as a function of albedo for cylindrical and tetrahedral hohlraums on OMEGA, for equal beam energies (“full power”) and for optimized relative beam energies (“tuned”). Each hohlraum is designed for optimum symmetry (at full power) at an albedo of 0.8. The cylindrical hohlraum is sensitive to large swings in the P_2 and P_4 Legendre modes and thus requires tuning, while the tetrahedral hohlraum is dramatically less sensitive to albedo. This is due to the uniform coverage of the hohlraum wall seen in Fig. 68.14 (Note that time-dependent tuning, not considered here, is needed for cylindrical hohlraums for optimum performance.)

tetrahedral hohlraum in comparison with that of the NIF (see below) is due in part to the absence on OMEGA of the Y_{20} spherical-harmonic component.

Tetrahedral Hohlraums on the NIF

Similar calculations have been performed for tetrahedral hohlraums on the NIF. The hohlraum dimensions are listed in Table 68.II. (The dimensions for cylindrical hohlraums are given for comparison, although results for cylindrical hohlraums are not given in this article.)

Figure 68.16(a) shows a sinusoidal plot of the NIF port locations for the most recent design. The ring of 12 beams at $\theta_5 = 77.45^\circ$ is provided to accommodate direct drive. The azimuthal angles between each of rings 1 through 4 and their reflections in the lower hemisphere are chosen so that beam dumps are located a quarter of a port spacing from the ports in the opposing rings. The relative azimuthal angle between rings 1 and 3 is chosen over other possibilities to give the configuration best suited to tetrahedral hohlraums. Specifically, the ϕ 's of the first beam port in each of the ten rings, from top to bottom, are $78.75^\circ, 33.75^\circ, 16.875^\circ, 39.375^\circ, 24.375^\circ, 5.625^\circ, 5.625^\circ, 28.125^\circ, 56.25^\circ,$ and 11.25° .

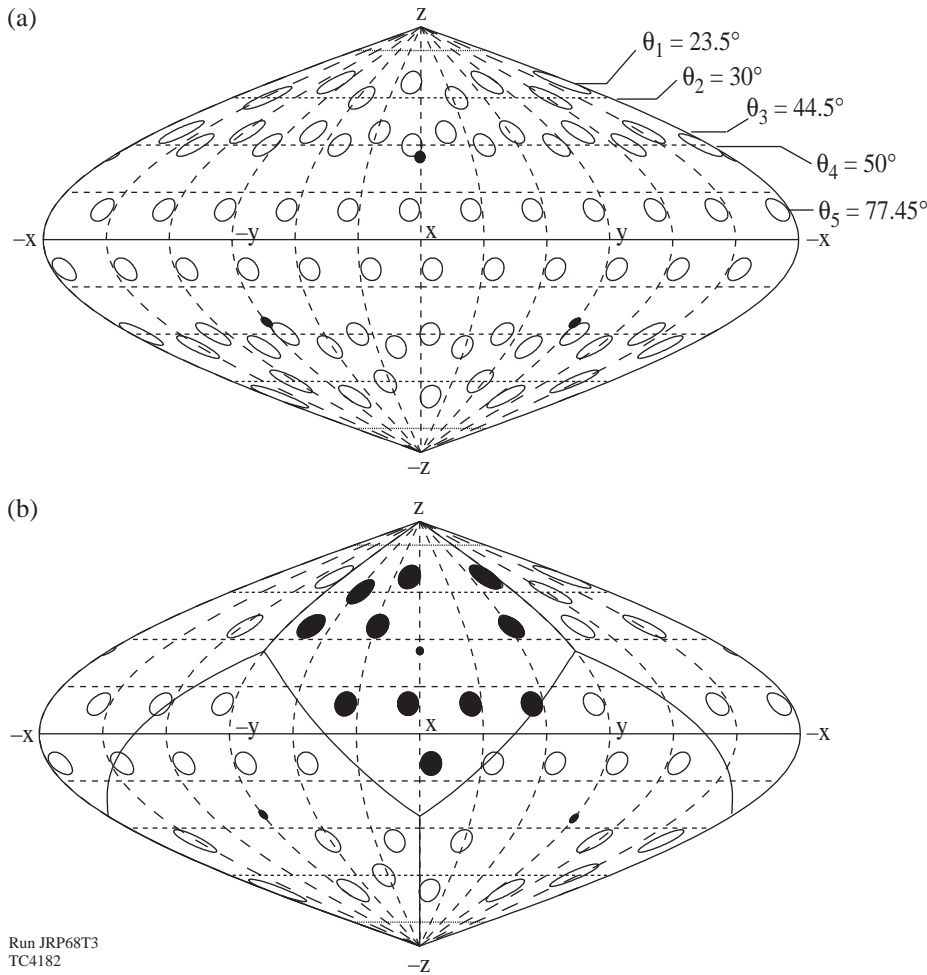


Figure 68.16

(a) Sinusoidal map of the proposed port locations on the NIF target chamber. Cylindrical hohlraums are irradiated with rings 1 through 4, and direct-drive targets with rings 1, 3, and 5. The small solid circles indicate LEH placements with $\theta_{\text{LEH}} = 55^\circ$. The subset used for tetrahedral hohlraums is shown in (b), which also divides the surface of the sphere into the four regions closest to each LEH.

Run JRP68T3
TC4182

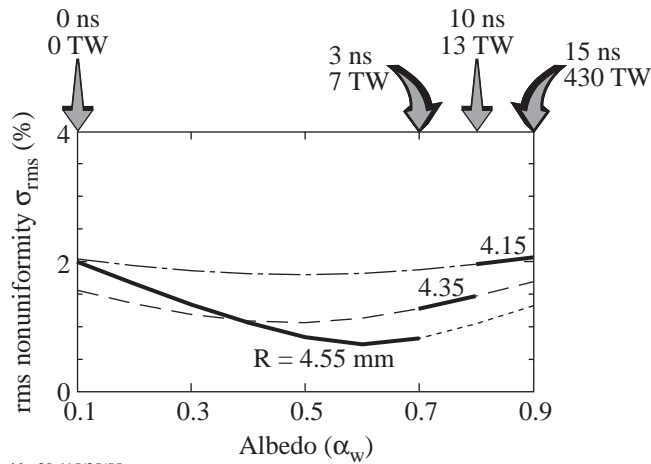
Figure 68.16(b) illustrates the surface of the sphere divided into the four sectors corresponding to tetrahedral symmetry. The LEH's are placed at the vertices of a true tetrahedron (i.e., $\theta_{\text{LEH}} = 55^\circ$). It is possible to use 11 out of the 12 available beams. It may be noted that one beam from the lower hemisphere is pointed into the LEH shown in the upper hemisphere. Each beam is directed into the closest LEH.

BUTTERCUP calculations for a representative design were carried out for three separate hohlraum radii: 4.55 to 4.15 mm, allowing for 0.4 mm of wall motion during the laser pulse (see Fig. 68.17). This is consistent with a 1-D *LASNEX* calculation.²¹ From the *LASNEX* calculation it was also possible to estimate the time and incident laser power corresponding to each value of albedo. These are indicated in Fig. 68.17, where the appropriate portions of the three curves are shown solid.

The rms nonuniformity σ_{rms} is close to 2% for all values of albedo. In this calculation time-independent tuning was used

(as in Fig. 68.15 for OMEGA). This resulted in an energy into the hohlraum of 1.3 MJ [out of the available untuned energy of 1.65 MJ ($11/12 \times 1.8$ MJ)]. However, with time-dependent tuning, significantly more than 1.3 MJ can be used because the tuning is only needed at early time (low albedo). Thus, if the hohlraum were tuned in a time-dependent way, i.e., during the rising part of the laser pulse but not during the final, maximum-power portion, close to 1.65 MJ would be delivered to the hohlraum and σ_{rms} would stay within 2% throughout the pulse.

The incidence angles of the 11 beams through the LEH are 23.0° , 23.7° , 31.5° , 32.2° , 39.2° , 43.6° , 47.2° , 47.8° , 53.8° , 53.9° , and 54.9° . Beam paths with the minimum and maximum angles are shown in Fig. 68.10. Some design flexibility is available by making minor adjustments to the (θ, ϕ) coordinates of the LEH and by not pointing some beams through the center of the LEH. However, experiments aimed at exploring clearance and symmetry issues in tetrahedral hohlraums are needed before such detailed design issues are addressed.



jds_20.415/35/55
TC4234

Figure 68.17

Nonuniformity σ_{rms} as a function of albedo for a NIF tetrahedral hohlraum. Wall motion is treated by assuming that the hohlraum radius reduces from 4.55 mm to 4.15 mm during the 15-ns laser pulse. The mapping shown between time (and power) in the laser pulse and albedo is obtained from a *LASNEX* calculation. The solid portions of the curves indicate the appropriate radius to use for σ_{rms} at a given time, based on the same *LASNEX* calculation.

Summary

A view-factor code has been developed to carry out a comparative study of indirect-drive uniformity in cylindrical and tetrahedral hohlraums. This code does not include hydrodynamics and radiation physics, but it has the merit of being fully 3-D. It has been used to model both types of hohlraum, for both the NIF and OMEGA laser systems.

The results for cylindrical hohlraums are in accord with what has been well established, namely that the P_2 nonuniformity is the dominant nonuniformity and must be compensated through varying the relative powers of the different laser beams as a function of time, a process known as beam phasing. Tetrahedral hohlraums, on the other hand, display a significantly reduced sensitivity to the changing wall albedo and may not require beam phasing at all if an rms nonuniformity around the capsule of 2% or less at all times is acceptable.

Examination of the NIF geometry has shown that, by appropriately using the extra beam ports proposed for direct drive, it is also possible to irradiate tetrahedral hohlraums on the NIF. Instead of diverting 24 of the 48 beams to the equatorial region of the target chamber, as for direct drive, one diverts 20 beams, all 8 beams from each of the rings at 50° and 2 beams from each of the rings at 30° , to the equator. On-capsule uniformity of $\sim 2\%$ throughout the pulse can be obtained. The main uncer-

tainty appears to relate to issues of clearance through the LEH's; this is a greater problem than for cylindrical hohlraums because some laser beams intersect the hohlraum wall close to the LEH's. Clearance of the capsule plasma is not significantly different in the two cases. While tuning may not be necessary for a tetrahedral hohlraum, appropriate tuning (which could be time independent on OMEGA and time dependent on the NIF) can enhance the uniformity with a minimal energy penalty.

Tetrahedral hohlraums have an intrinsically better uniformity than cylindrical hohlraums, but suffer the disadvantages of being fully 3-D, harder to model, and harder to diagnose experimentally. However, with advances in modeling and diagnostic capabilities, these disadvantages may become minor. At the very least, tetrahedral hohlraums merit consideration as an alternative route to indirect-drive ignition and gain on the NIF. The OMEGA laser is ideally suited to carry out proof-of-principle experiments on tetrahedral hohlraums. The first such experiments are being planned in collaboration with the Los Alamos National Laboratory and the Lawrence Livermore National Laboratory.

More details on the work reported in this article can be found in Ref. 22.

ACKNOWLEDGMENT

The authors are pleased to acknowledge many detailed discussions with Dr. S. M. Pollaine over an extended period of time. The interest of Dr. D. Eimerl and Dr. M. D. Rosen has also been greatly appreciated. This work was supported by the U.S. Department of Energy Office of Inertial Confinement Fusion under Cooperative Agreement No. DE-FC03-92SF19460, the University of Rochester, the New York State Energy Research and Development Authority, and by the Laboratory for Laser Energetics Summer High-School Research Program, supported by National Science Foundation Contract No. ESI9256079.

REFERENCES

- (a) Also J. C. Wilson Magnet High School, Rochester, NY 14611. Current address: Harvard University, Cambridge, MA 02138.
1. J. Lindl, *Phys. Plasmas* **2**, 3933 (1995).
2. A. A. Hauer *et al.*, *Phys. Plasmas* **2**, 2488 (1995).
3. L. J. Suter *et al.*, *Phys. Rev. Lett.* **73**, 2328 (1994).
4. S. W. Haan *et al.*, *Phys. Plasmas* **2**, 2480 (1995).
5. S. E. Bodner, *Comments Plasma Phys. Control. Fusion* **16**, 351 (1995).
6. N. D. Delamater *et al.*, *Phys. Plasmas* **3**, 2022 (1996).
7. D. W. Phillion and S. M. Pollaine, *Phys. Plasmas* **1**, 2963 (1994).

8. H. Azechi *et al.*, Jpn. J. Appl. Phys. **20**, L477 (1981).
9. C. Yamanaka *et al.*, in *Plasma Physics and Controlled Nuclear Fusion Research 1984* (IAEA, Vienna, 1985), Vol. 3, p. 3.
10. Y. Kato *et al.*, in *Plasma Physics and Controlled Nuclear Fusion Research 1990* (IAEA, Vienna, 1991), Vol. 3, p. 89.
11. T. Mochizuki, S. Sakabe, and C. Yamanaka, Jpn. J. Appl. Phys. **22**, L124 (1983).
12. M. Murakami and K. Nishihara, Jpn. J. Appl. Phys. **25**, 242 (1986).
13. D. C. Wilson *et al.*, Bull. Am. Phys. Soc. **35**, 2021 (1990).
14. M. Murakami and J. Meyer-ter-Vehn, Nucl. Fusion **31**, 1333 (1991).
15. M. Murakami and J. Meyer-ter-Vehn, Nucl. Fusion **31**, 1315 (1991).
16. G. D. Tsakiris, Phys. Fluids B **4**, 992 (1992).
17. M. Murakami, Nucl. Fusion **32**, 1715 (1992).
18. R. L. Kauffman *et al.*, Phys. Rev. Lett. **73**, 2320 (1994).
19. M. D. Cable *et al.*, Phys. Rev. Lett. **73**, 2316 (1994).
20. Ya. B. Zel'dovich and Yu. P. Raizer, in *Physics of Shock Waves and High-Temperature Hydrodynamic Phenomena*, edited by W. D. Hayes and R. F. Probstein (Academic Press, New York, 1966), Vol. I, p. 131.
21. S. M. Pollaine, private communication (1996).
22. J. D. Schnittman and R. S. Craxton, Phys. Plasmas **3**, 3786 (1996).